Supporting Information

Multi-layered Mesoporous TiO$_2$ Thin Films with Large Pore and Highly Crystalline Frameworks for Efficient Photoelectrochemical Conversion

Dan Feng[a], Wei Luo[a], Junyong Zhang[a], Ming Xu[a], Renyuan Zhang[a], Haoyu Wu[a], Yingying Lv[a], Abdullah M. Asiri[b], Sher Bahader Khan[b], Mohammed M. Rahman[b], Gengfeng Zheng[a]*, and Dongyuan Zhao[a]*

[a] Department of Chemistry, Shanghai Key Laboratory of Molecular Catalysis and Innovative Materials, Laboratory of Advanced Materials, Fudan University, Shanghai 200433, P. R. China.

[b] Chemistry Department and The Center of Excellence for Advanced Materials Research, King Abdul-Aziz University, P.O. Box 80203, Jeddah 21589, Saudi Arabia.

Email: dyzhao@fudan.edu.cn; gfzheng@fudan.edu.cn; Tel: +86-21-5163-0205, Fax: +86-21-5163-0307
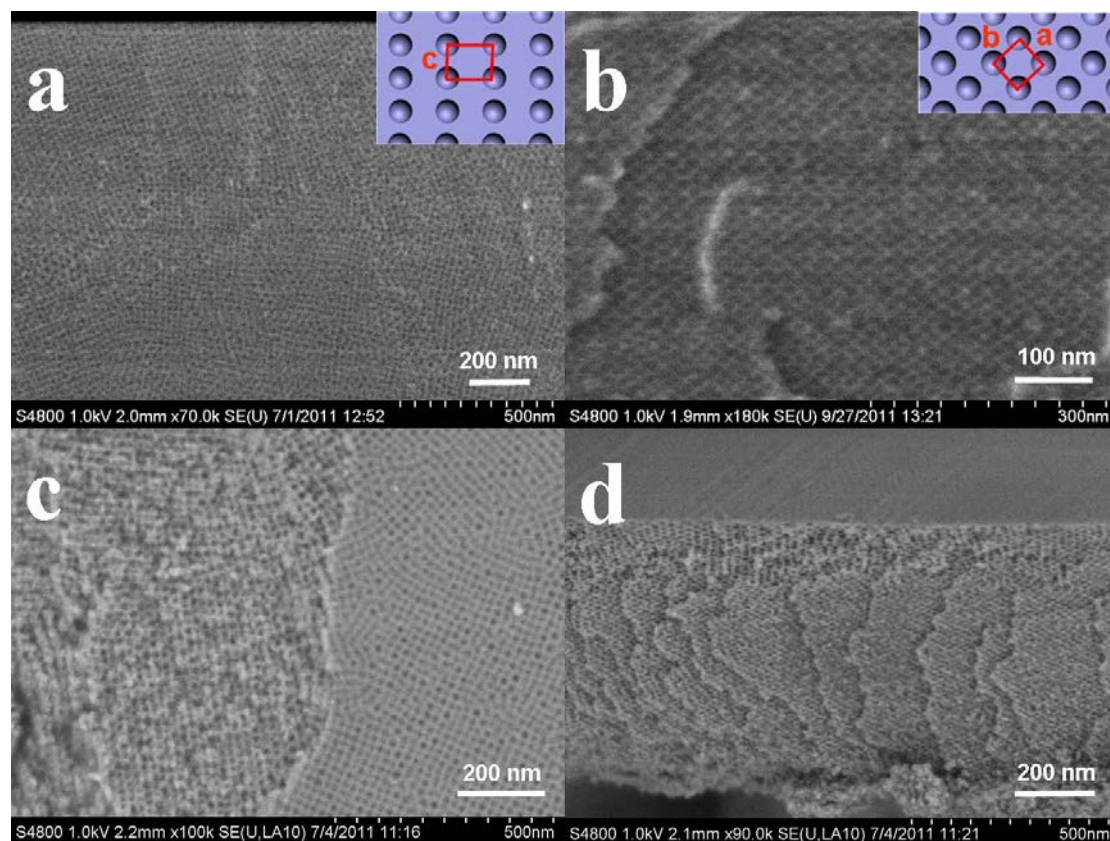
Fig. S1 SEM images of (a, b) as-deposited mesostructured TiO$_2$/surfactant composite films aged at 100 °C and (c, d) mesoporous TiO$_2$ films after pyrolysis in nitrogen at 500 °C. Images (a) and (c) showing top surfaces and edge parts of the films, while (b) and (d) showing the cross-section images of the films.
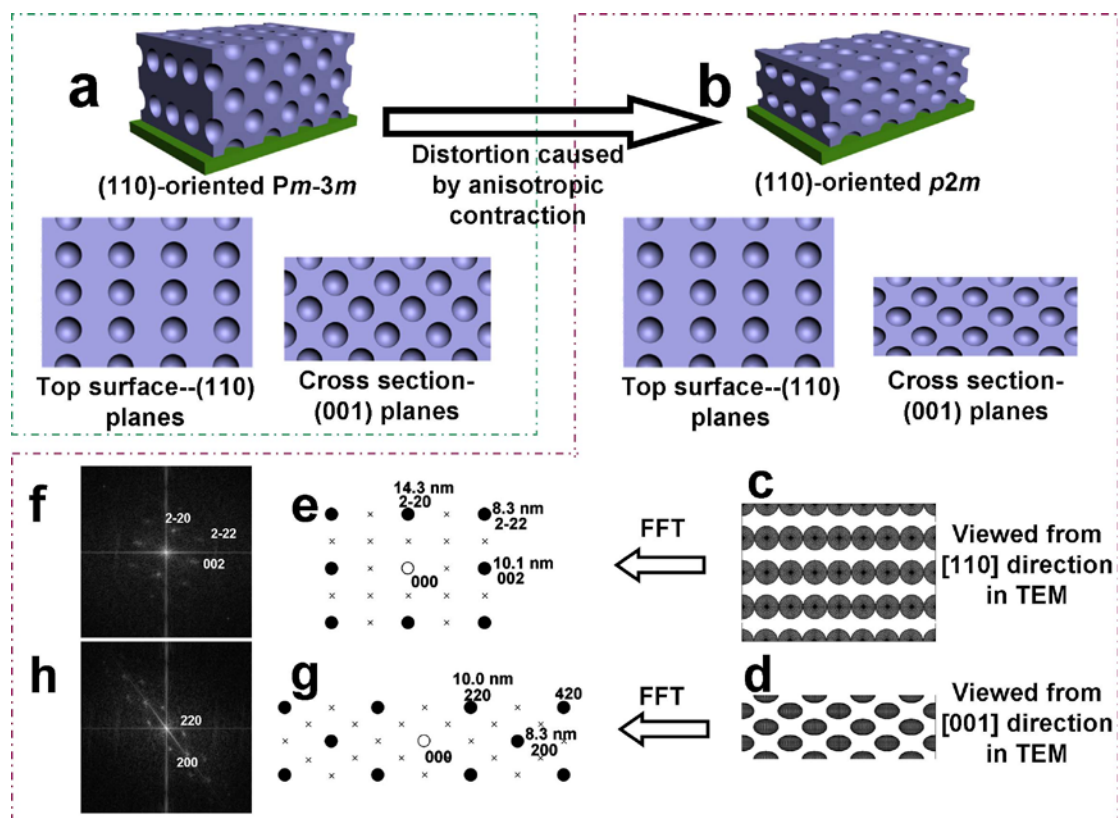
Fig. S2 Schematic representation of the structural conversion of the mesoporous TiO_2 films from (a) a (110)-oriented primitive cubic $Pm\bar{3}m$ structure to (b) a monoclinic $p2m$ structure during the pyrolysis. (a, b) are simulated models of the morphologies of films on substrates, top surfaces and cross-sections corresponding to the SEM images; (c, d) are simulated perspective figures of the pyrolyzed film corresponding to the TEM images viewed from [110] and [001] directions, respectively; (e – h) are indexed FFT patterns and schematic representations according to the TEM images in Figure 1e and 1f.
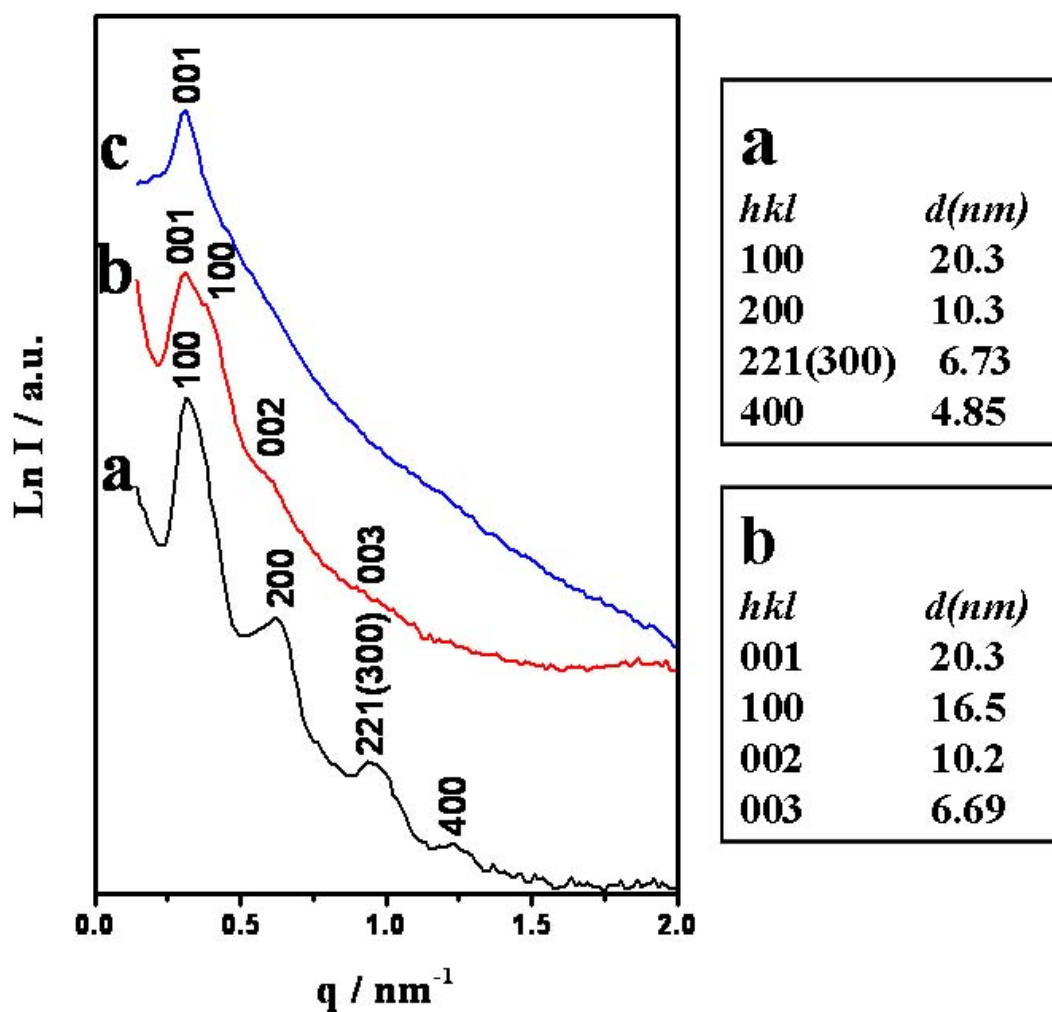
a

hkl	d(nm)
100	20.3
200	10.3
221(300)	6.73
400	4.85

b

hkl	d(nm)
001	20.3
100	16.5
002	10.2
003	6.69

Fig. S3 SAXS patterns of (a) as-deposited TiO_2/surfactant composite films aged at 100 °C, (b) the mesoporous TiO_2 films after pyrolysis in nitrogen at 500 °C, and (c) mesoporous pure TiO_2 films after pyrolysis in air at 450 °C.
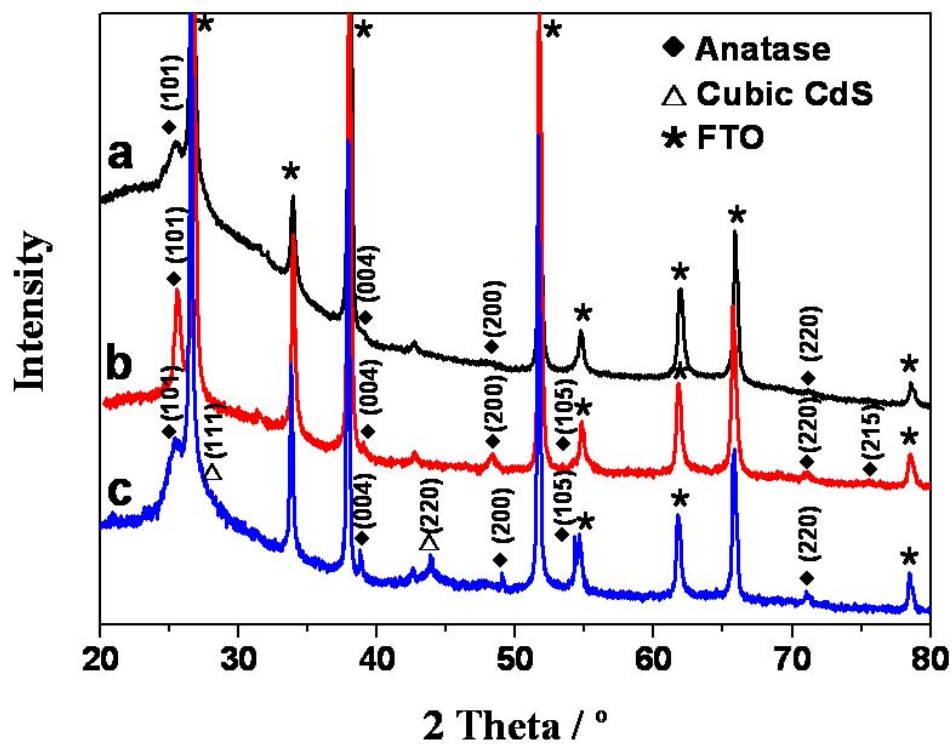
Fig. S4 Wide-angle XRD patterns of the highly ordered mesoporous TiO_2 films (a) after pyrolysis in nitrogen at 500 °C, (b) after pyrolysis in air at 450 °C, and (c) after doped with CdS QDs-sensitization.
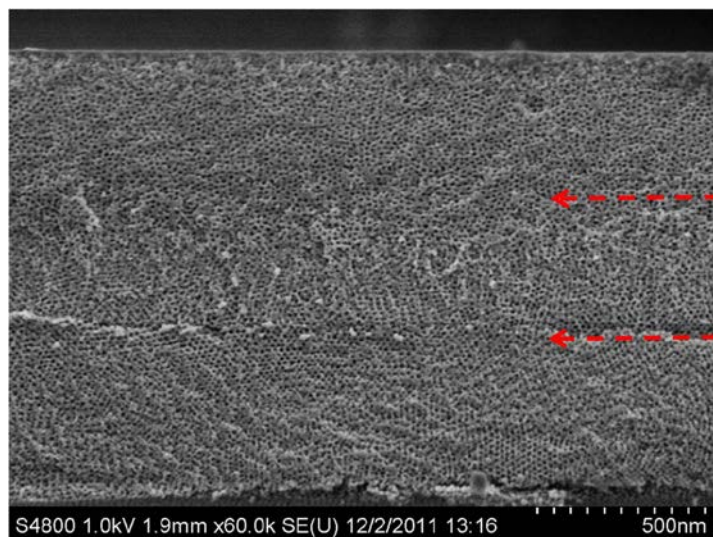
Fig. S5 The cross-section SEM image of the 3-layered mesoporous TiO_2-3L films (with thickness of 1700 nm) by coating 3 times.

Fig. S6 (a) Top surface view SEM image and (b) EDX pattern of the CdS QDs-sensitized mesoporous TiO$_2$ film.
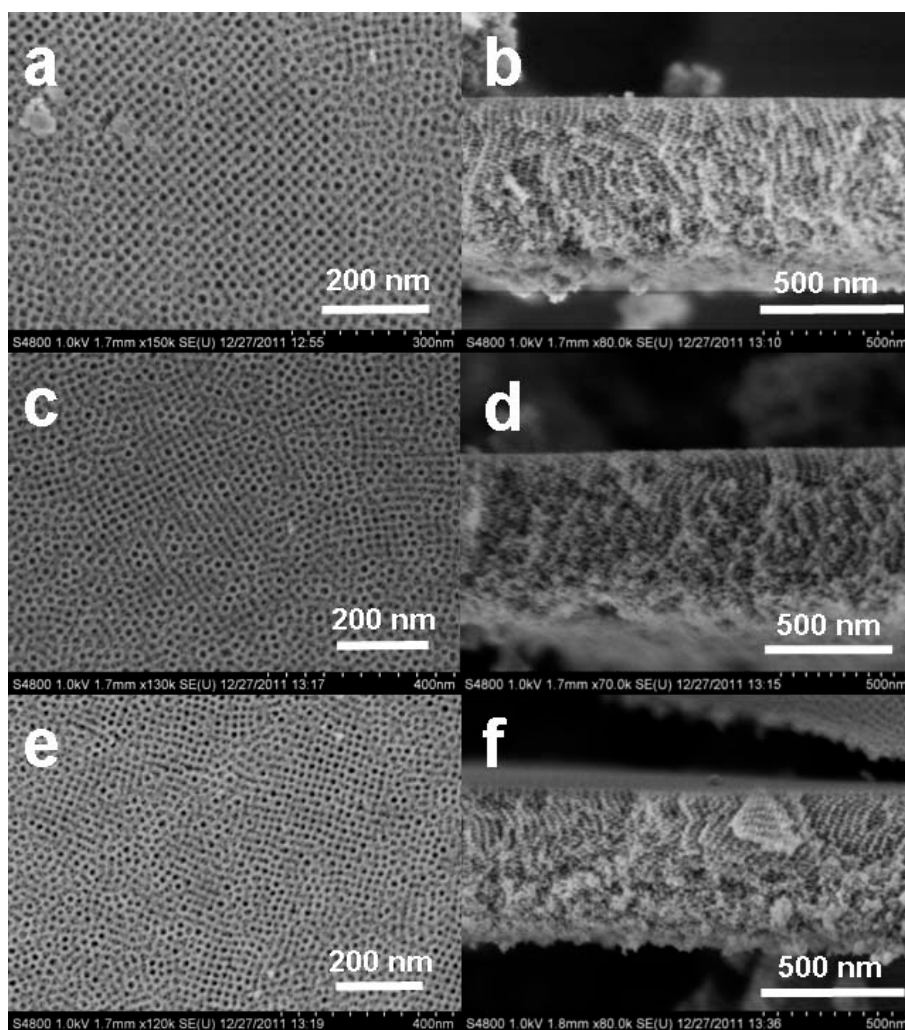
Fig. S7 SEM images of (a, b) Cr-doped, (c, d) Ni-doped, and (e, f) Co-doped mesoporous TiO₂ films after being pyrolyzed at 500 °C in nitrogen and in air at 450 °C. The metal/Ti atomic ratio is ~ 2.0 %.
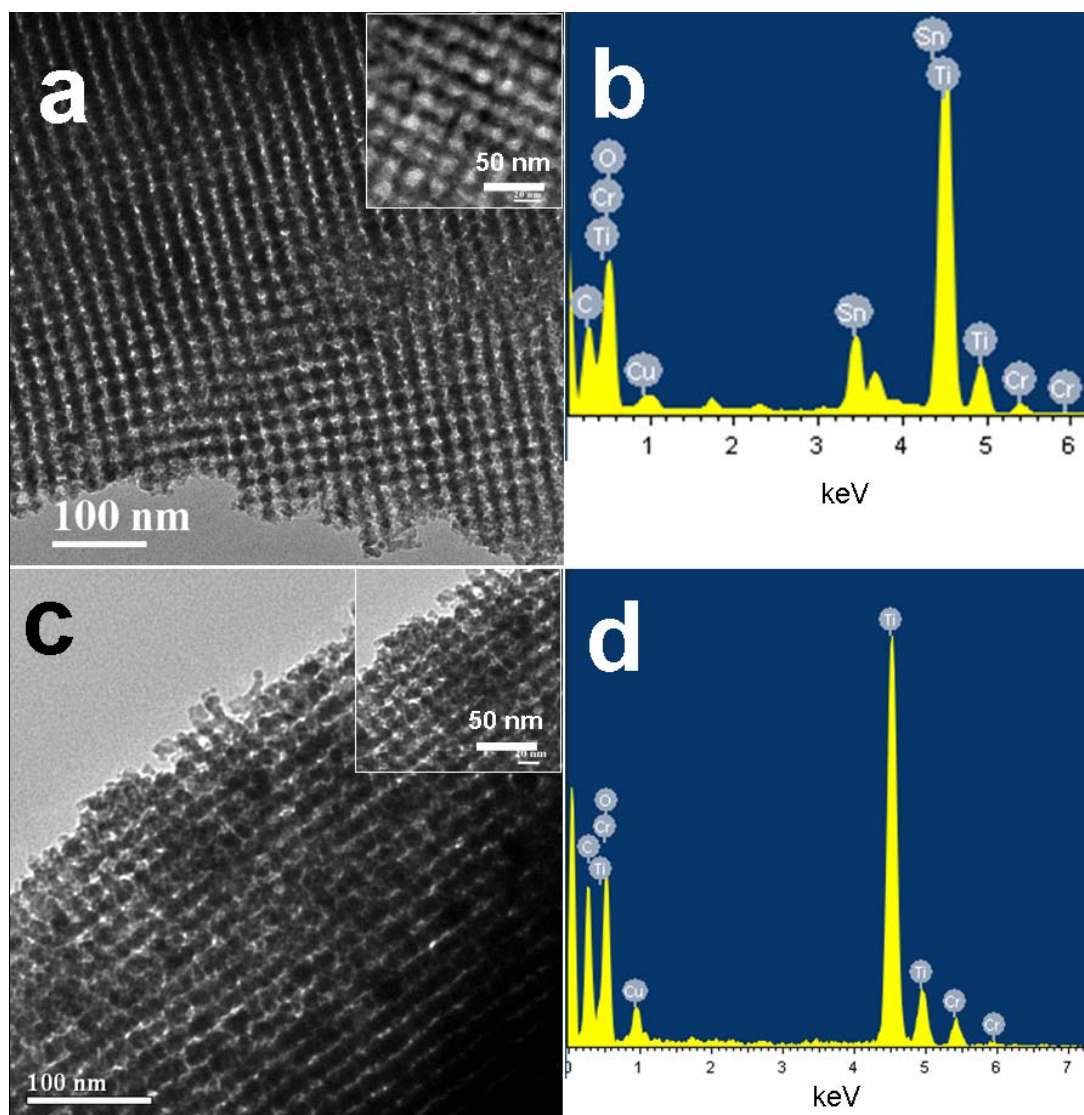
Fig. S8 TEM images and EDX patterns of the Cr-doped mesoporous TiO$_2$ films with Cr/Ti atomic ratio of ~ 2.0 % (a, b) and ~ 6.0 % (c, d).
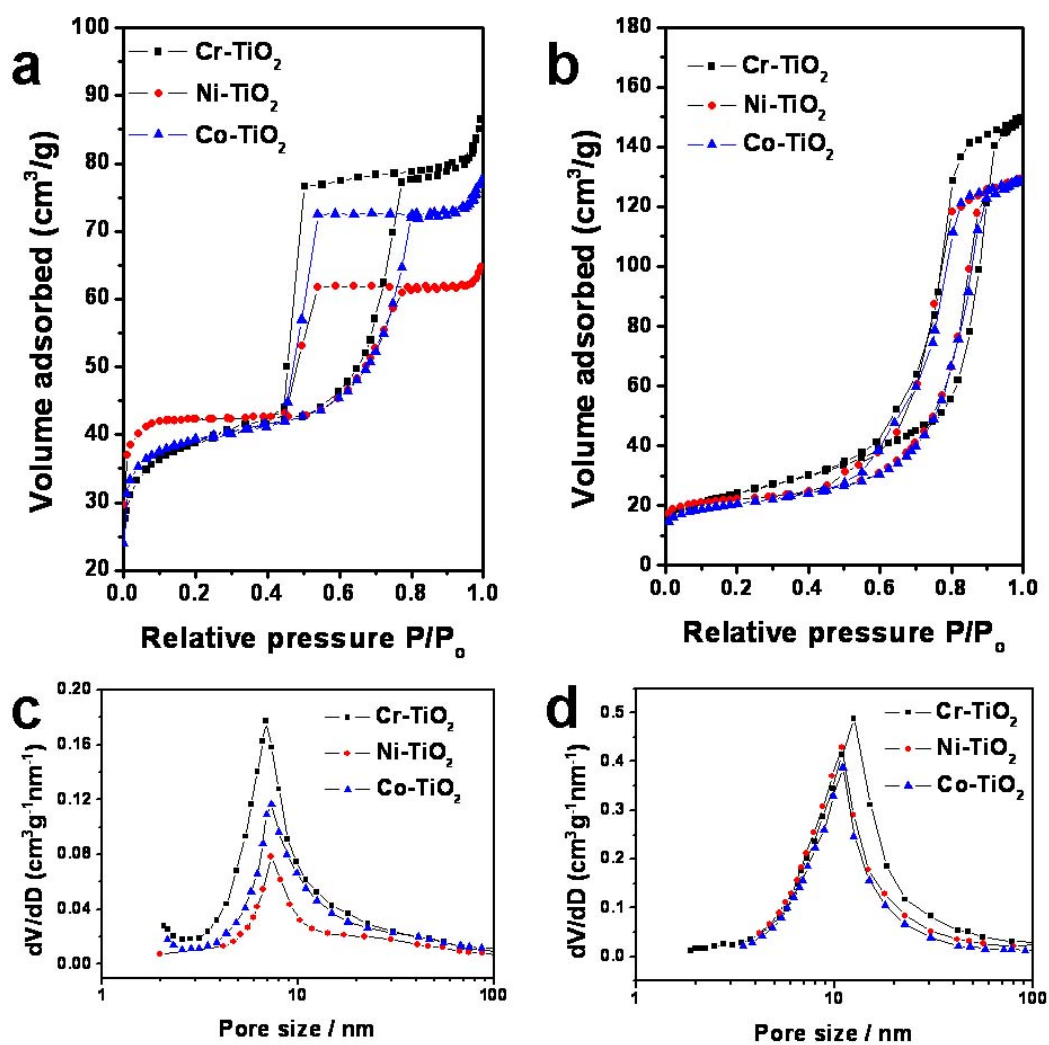
Fig. S9 (a, b) Nitrogen sorption isotherms and (c, d) pore size distributions of Cr-doped, Ni-doped, and Co-doped mesoporous TiO$_2$ films with a metal/Ti atomic ratio of 2.0 % after pyrolysis at 500 °C in nitrogen and in air at 450 °C.
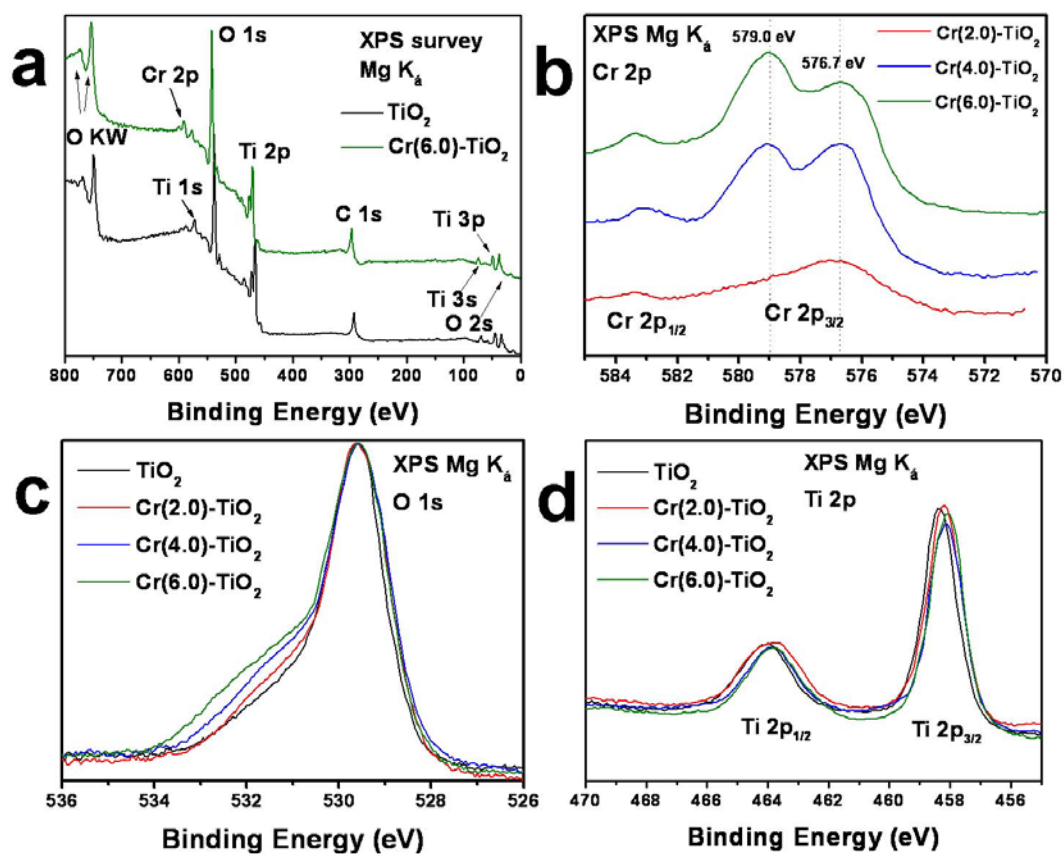
Fig. S10 (a) XPS survey spectra, (b) Cr 2p XPS spectra, (c) normalized O 1s XPS spectra and (d) Ti 2p XPS spectra of the mesoporous TiO_2 films and Cr-doped mesoporous TiO_2 films including $Cr(2.0)-TiO_2$, $Cr(4.0)-TiO_2$ and $Cr(6.0)-TiO_2$ films with a Cr /Ti atomic ratio of 2.0, 4.0 and 6.0 %, respectively.
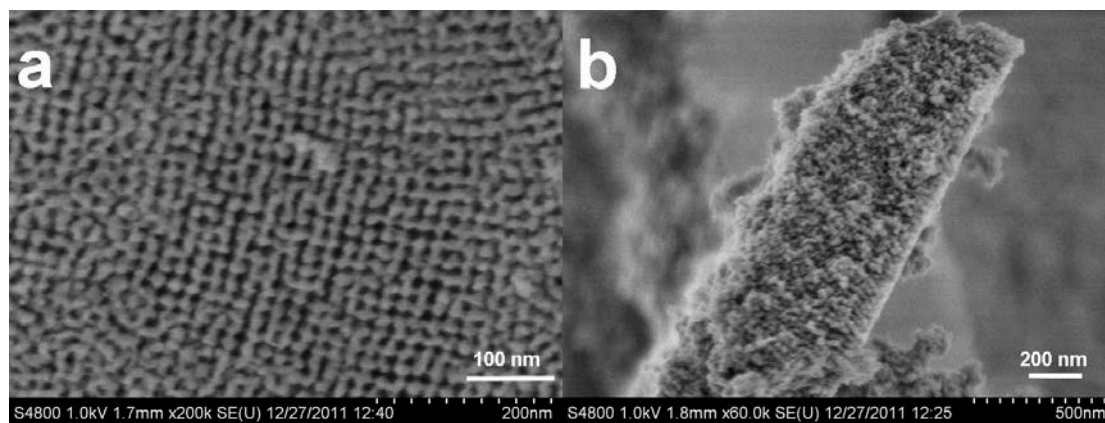
Fig. S11 SEM images of (a) top surface and (b) cross section view of the Cr-doped mesoporous TiO_2 films with a Cr/Ti atomic ratio of ~ 6.0 % after pyrolysis at 500 °C in nitrogen and in air at 450 °C.
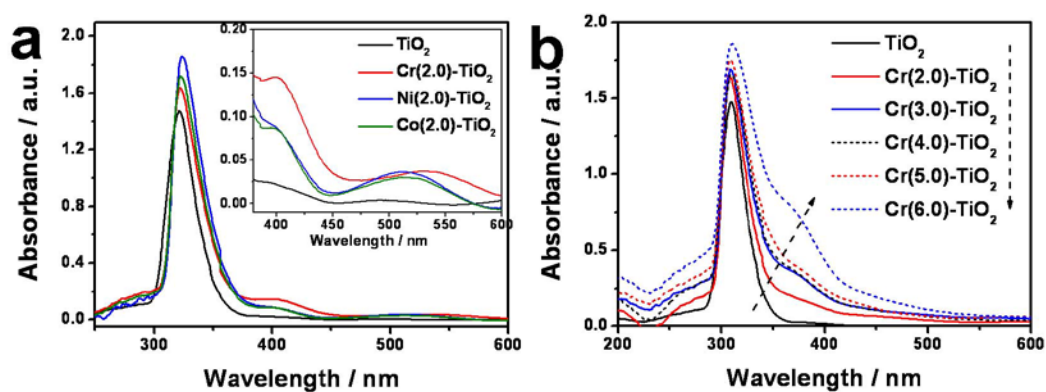
Fig. S12 UV-vis absorption spectra of (a) different metal ions doped mesoporous TiO_2 film with a metal/Ti atomic ratio of ~ 2.0 % and (b) Cr-doped mesoporous TiO_2 films with different Cr /Ti atomic ratios of 0, 2.0, 3.0, 4.0, 5.0 and 6.0 %, respectively. Inset (a) is magnified part of the adsorption spectra in the range of 375 to 600 nm.

Fig. S13 Photocatalytic degradation of rhodamine B (RhB) using film based devices by placing mesoporous TiO_2 films and Cr-doped mesoporous TiO_2 films including Cr(2.0)-TiO_2, Cr(4.0)-TiO_2 and Cr(6.0)-TiO_2 films with a Cr /Ti atomic ratio of 2.0, 4.0 and 6.0 %, respectively. (a) 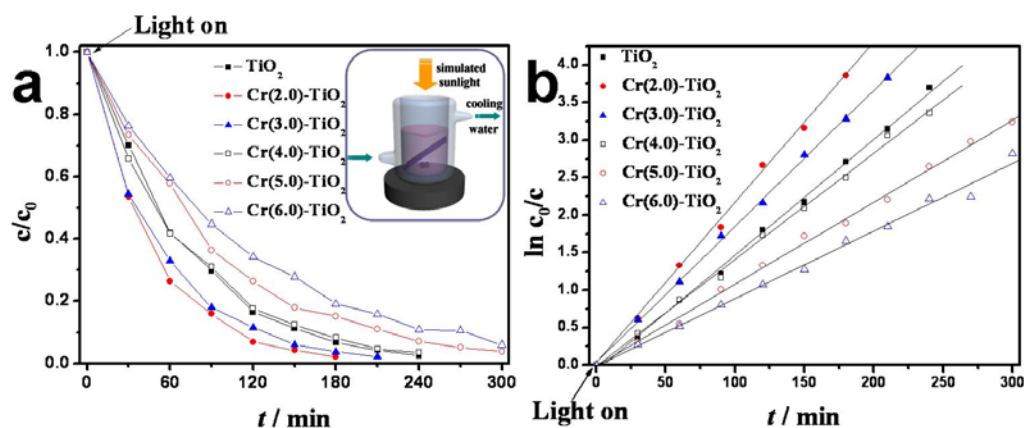Dye concentration change versus irradiation time and (b) ln c_0/c versus irradiation time (dots) and the linear fits (lines). Inset in (a) is the schematic illustration of experimental. The photocatalytic performance of the Cr-doped mesoporous TiO_2 film was evaluated by the photocatalytic degradation of RhB under simulated sunlight illuminated by a 300 W Xe lamp and at ambient condition. The film samples with substrates (film area of 2×2 cm^2) were directly placed into a quartz vessel containing 12 mL RhB aqueous solution (1×10^{-5} mol/L). Before illumination, the reaction system was placed in dark for 30 min to ensure the adsorption balance of RhB molecules by the mesoporous films. The variation of concentration was monitored by the *in situ* UV-vis quantitative analysis at the maximum adsorption wavelength of RhB (552 nm). Cooling water was used to avoid water evaporation.
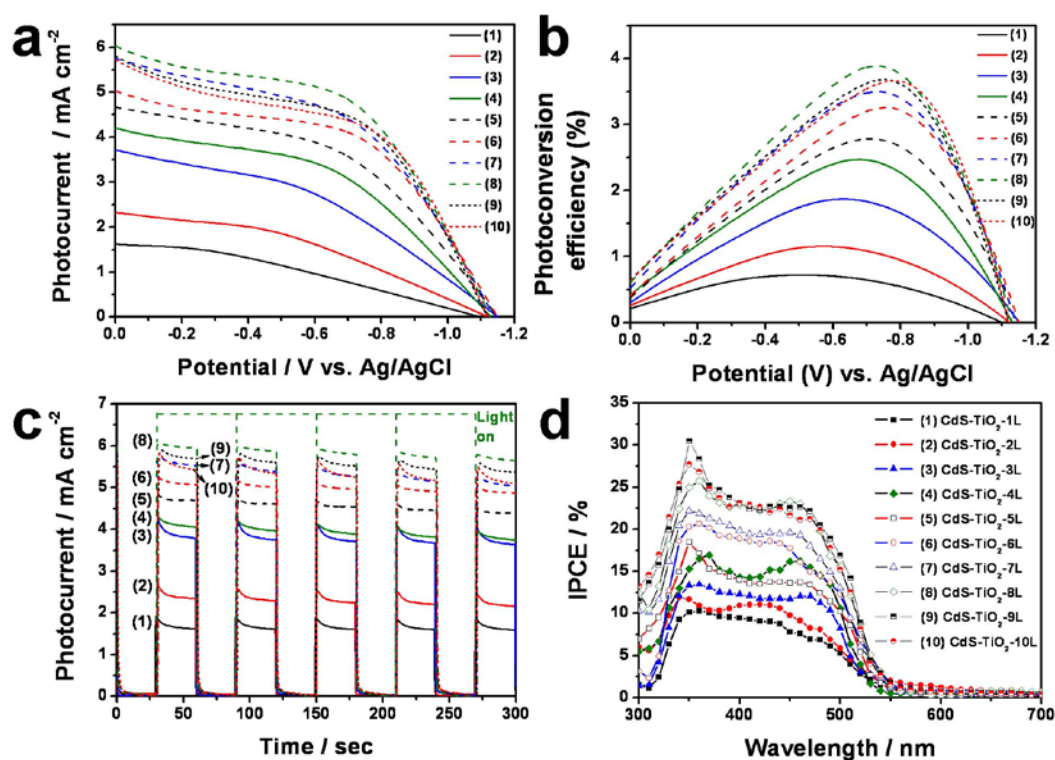
Fig. S14 (a) Photocurrent *versus* voltage characteristics, (b) calculated photoconversion efficiencies, (c) current *versus* time measurements and (d) IPCE spectra of the CdS-sensitized mesoporous TiO_2 films including (1) CdS-TiO_2-1L, (2) CdS-TiO_2-2L, (3) CdS-TiO_2-3L, (4) CdS-TiO_2-4L, (5) CdS-TiO_2-5L, (6) CdS-TiO_2-6L, (7) CdS-TiO_2-7L, (8) CdS-TiO_2-8L, (9) CdS-TiO_2-9L and (10) CdS-TiO_2-10L with 1–10 layers, respectively.
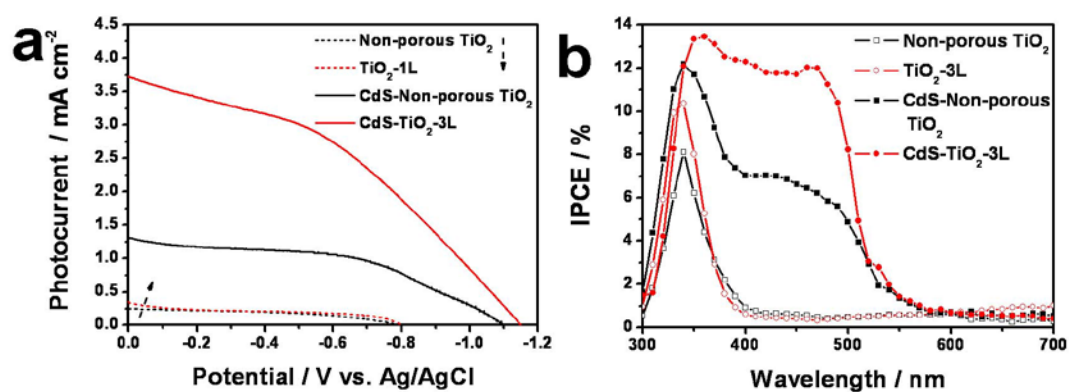
Fig. S15 (a) Photocurrent *versus* voltage characteristics and (b) IPCE spectra of the control non-porous TiO_2 film sample (with the thickness of ~ 1850 nm), the 3-layered mesoporous TiO_2 film (TiO_2-3L, thickness of ~ 1700 nm), the CdS-sensitized non-porous TiO_2 film (thickness of 1850 nm) and the CdS-sensitized mesoporous TiO_2 film (CdS-TiO_2-3L, thickness of 1700 nm).

Table S1. PEC performance parameters of the highly-ordered mesoporous TiO_2 films with different thicknesses and corresponding CdS-sensitized mesoporous TiO_2 films.[a]

Sample	Thickness / nm	J_{sc} / mA/cm^2	V_{oc} / V	η / %
TiO_2-1L	500	0.14	–0.77	0.04
TiO_2-2L	1100	0.23	–0.78	0.17
TiO_2-3L	1700	0.35	–0.80	0.18
Non-porous TiO_2-3L	1850	0.25	–0.80	0.17
CdS-TiO_2-1L	500	1.62	–1.10	0.72
CdS-TiO_2-2L	1100	2.33	–1.12	1.53
CdS-TiO_2-3L	1700	3.72	–1.15	1.87
CdS-Non-porous TiO_2-3L	1850	1.31	–1.10	0.80
CdS-TiO_2-4L	2250	4.21	–1.13	2.47
CdS-TiO_2-5L	2900	4.67	–1.15	2.79
CdS-TiO_2-6L	3500	5.03	–1.15	3.26
CdS-TiO_2-7L	4050	5.75	–1.14	3.50
CdS-TiO_2-8L	4750	6.03	–1.13	3.89
CdS-TiO_2-9L	5350	5.81	–1.12	3.68
CdS-TiO_2-10L	5800	5.72	–1.12	3.67

[a] The denotation: "TiO_2-xL" represents the mesoporous TiO_2 film with x layers obtained by coating x times and the corresponding CdS-sensitized film names "CdS-TiO_2-xL". The thickness of the resultant mesoporous TiO_2 films was measured by Surface Profiler. The short circuit currents (J_{sc}) were measured at 0 V (*vs.* Ag/AgCl). The open-circuit photovoltages (V_{oc}) are values *versus* Ag/AgCl electrode. Photoconversion efficiencies (η) refer the optimal conversion efficiencies calculated based on the *I-V* measurements.

Table S2. Porosities of the mesoporous TiO_2 and metal-doped mesoporous TiO_2 films.[a]

Sample	D / nm	D_w / nm	V_t /cm^{3}g^{-1}	S_{BET} / m^{2}g^{-1}
TiO_2-500N	8.0	4.0	0.18	161
Cr(2.0)-TiO_2-500N	6.9	3.8	0.13	136
Ni(2.0)-TiO_2-500N	7.2	4.0	0.10	152
Co(2.0)-TiO_2-500N	7.3	3.9	0.12	137
TiO_2-500N-450A	13.0	7.5	0.25	102
Cr(2.0)-TiO_2-500N-450A	12.5	7.6	0.25	85
Ni(2.0)-TiO_2-500N-450A	10.9	7.7	0.21	77
Co(2.0)-TiO_2-500N-450A	11.0	7.7	0.21	72

[a] The "500N" and "450A" in sample names refer to the pyrolysis conditions at 500 °C in nitrogen and at 450 °C in air, respectively. Pore diameter calculated by the Barrett-Joyner-Halenda (BJH) method using adsorption branches. Window size calculated by the Barrett-Joyner-Halenda (BJH) method using desorption branches. Total pore volume calculated as the amount of nitrogen adsorbed at a relative pressure of 0.995.